CO_2 flux over young and snow-covered Arctic pack ice in winter and spring

Daiki Nomura[1, 2, 3*], Mats A. Granskog[4], Agneta Fransson[4], Melissa Chierici[5, 6], Anna Silyakova[7], Kay I. Ohshima[1, 3], Lana Cohen[4], Bruno Delille[8], Stephen R. Hudson[4], and Gerhard S. Dieckmann[9]

1 Institute of Low Temperature Science, Hokkaido University, Kita–19, Nishi–8, Kita–ku, Sapporo, Hokkaido 060–0819, Japan.

2 Faculty of Fisheries Sciences, Hokkaido University, 3–1–1, Minato–cho, Hakodate, Hokkaido 041–8611, Japan.

3 Arctic Research Center, Hokkaido University, Kita–21, Nishi–11, Kita–ku, Sapporo, Hokkaido 001–0021, Japan.

4 Norwegian Polar Institute, Fram Centre, NO–9296 Tromsø, Norway.

5 Institute of Marine Research, NO–9294, Tromsø, Norway.

6 FRAM-High North Research Centre for Climate and the Environment, Tromsø, Norway.

7 CAGE, Centre for Arctic Gas Hydrate, Environment and Climate, Tromsø, Norway.

8 Unité d'Océanographie Chimique, Freshwater and OCeanic science Unit of research, Université de Liège, Liège, Belgium.

9 Alfred Wegener Institute for Polar and Marine Research, Bremerhaven, Germany.

＊Corresponding author: Daiki Nomura, e-mail: daiki.nomura@fish.hokudai.ac.jp,
Faculty of Fisheries Sciences, Hokkaido University, 3–1–1, Minato–cho, Hakodate,
Hokkaido 041–8611, Japan.

Abstract

Rare CO_2 flux measurements from Arctic pack ice show that two types of ice contribute to the release of CO_2 from the ice to the atmosphere during winter and spring: young, thin ice with a thin layer of snow, and older (several weeks), thicker ice with thick snow cover. Young, thin sea ice is characterized by high salinity and high porosity, and snow-covered thick ice remains relatively warm (>–7.5°C) due to the insulating snow cover despite air temperatures as low as –40°C. Therefore, brine volume fractions of these two ice types are high enough to provide favorable conditions for gas exchange between sea ice and the atmosphere even in mid-winter. Although the potential CO_2 flux from sea ice decreased due to the presence of the snow, the snow surface is still a CO_2 source to the atmosphere for low snow density and thin snow conditions. We found that young sea ice that is formed in leads without snow cover produces CO_2 fluxes an order of magnitude higher than those in snow-covered older ice (+1.0 ± 0.6 mmol C m^{-2} day^{-1} for young ice, and +0.2 ± 0.2 mmol C m^{-2} day^{-1} for older ice).

1 Introduction

Arctic sea ice is changing dramatically, with rapid declines in summer sea ice extent and a shift towards younger and thinner first-year ice rather than thick multi-year ice (e.g., Stroeve et al., 2012; Meier et al., 2014; Lindsay and Schweiger, 2015). Although the effects of sea ice formation and melting on biogeochemical cycles in the ocean have previously been discussed (e.g., Vancoppenolle et al., 2013), the effects of sea ice freeze and melt processes on carbon dioxide (CO_2) exchange with the atmosphere are still largely unknown (Parmentier et al., 2013).

Recent CO_2 flux measurements on sea ice indicate that sea ice is an active component in gas exchange between ocean and atmosphere (Nomura et al., 2013; Geilfus et al., 2013; 2014; Delille et al., 2014; Brown et al., 2015; Kotovitch et al., 2016). The sea-ice CO_2 fluxes depend on (a) the difference in the partial pressure of CO_2 (pCO_2) between the

sea ice surface and air, (b) brine volume fraction at the ice-snow interface, (c) ice surface condition including the snow deposited on ice, and (d) wind-driven pressure pumping through the snow. For (a), it is known that the air–sea ice CO_2 flux is driven by the differences in pCO_2 between the sea ice surface and atmosphere (e.g. Delille et al., 2014; Geilfus et al., 2014). Brine pCO_2 changes due to processes within the sea ice, such as thermodynamic process (e.g., Delille et al., 2014), biological activity (e.g., Delille et al., 2007; Fransson et al., 2013; Rysgaard et al., 2013), and calcium carbonate ($CaCO_3$; ikaite) formation and dissolution (e.g., Papadimitriou et al., 2012). When pCO_2 in brine is higher than that of air pCO_2, brine has the potential to release CO_2 to the atmosphere. Brine volume fraction (b) controls the permeability of sea ice (Golden et al. 1998) and thus CO_2 fluxes (Delille et al. 2014; Geilfus et al 2014). The air–sea ice CO_2 flux is also strongly dependent on the sea ice surface conditions (c) (Nomura et al., 2010a, 2013; Geilfus et al., 2013; 2014; Barber et al., 2014; Brown et al., 2015; Fransson et al., 2015). Nomura et al. (2013) proposed that snow properties (e.g., water equivalent) are important factors affecting gas exchange processes on sea ice. In addition, frost flowers (vapor-deposited ice crystals that wick brine from the sea ice surface) promote CO_2 flux from the ice to the atmosphere (Geilfus et al., 2013; Barber et al., 2014; Fransson et al., 2015). Finally, for (d), it is thought that CO_2 flux is affected by wind pumping through the snow pack (Massman et al.,1995; Takagi et al., 2005) in which the magnitude of CO_2 flux through snow or underlying soil (e.g., Takagi et al., 2005) can increase the transport relative to molecular diffusion by up to 40% (Bowling and Massman, 2011). These results were mainly found over land-based snow (soil and forest), and thus they are still poorly understood over sea ice (Papakyriakou and Miller, 2011).

In addition to the processes described above, the CO_2 flux over sea ice may also be influenced by the temperature difference between the ice surface and the atmosphere. This has been shown in previous studies in dry snowpacks over land surfaces. These studies show that there is an unstable air density gradient due to heating at the bottom producing a strong temperature difference between the bottom and top of the snowpack (e.g., Powers et al., 1985; Severinghaus et al., 2010). This produces air flow within the snowpack, which is a potentially significant contributor to mixing and transport of gas

and heat within the snowpack. We expect that this process would also occur in snow over sea ice, especially during the wintertime when air temperatures are coldest and the temperature difference between sea ice surface (snow bottom) and atmosphere is largest (e.g., Massom et al., 2001). Generally, the sea ice surface under thick snow cover is warm due to the heat conduction from the bottom of sea ice and the insulating effect of the snow cover, and a strong temperature difference between the sea ice surface and atmosphere is observed (e.g., Massom et al., 2001). Such a temperature difference would produce an unstable air density gradient and upward transport of air containing CO_2 degassed at the sea-ice surface, thereby enhancing CO_2 exchange between sea ice and atmosphere.

In the ice-covered Arctic Ocean, storm periods which produce high wind speeds and open leads are also important for air-to-sea CO_2 fluxes (Fransson et al., 2017) due to the under-saturation of the surface waters in CO_2 with respect to the atmosphere. In addition, the subsequent ice growth and frost flower formation in open leads promote ice-to-air CO_2 fluxes in winter (e.g. Barber et al., 2014). Given the fact that Arctic sea ice is shrinking and shifting from multi-year ice to first-year ice (e.g., Stroeve et al., 2012; Meier et al., 2014; Lindsay and Schweiger, 2015), the area of open ocean and thinner seasonal ice is increasing. Thus, a potential consequence may be increased contribution of open ocean surface and/or thinner sea ice to the overall CO_2 fluxes of the Arctic Ocean. The dynamics of the thinner ice pack, through formation of leads and new ice, will play an important role in the gas fluxes from the ice pack. However, there is a definite lack of information on sea ice processes during wintertime due to the difficulty in acquiring observations in winter pack ice, as reflected by the fact that most of the previous winter CO_2 flux measurements have been take over landfast ice.

The Norwegian young sea ICE (N-ICE2015) campaign in winter and spring 2015 provided opportunities to examine CO_2 fluxes between sea ice and atmosphere in a variety of snow and ice conditions in pack ice north of Svalbard. Formation of leads and their rapid refreezing allowed us to examine air–sea ice CO_2 fluxes over thin young sea ice, occasionally covered with frost flowers in addition to the snow-covered older ice that covers most of the pack ice area. The objectives of this study were to understand

the effects of i) thin sea ice and frost flower formation on the air–sea ice CO_2 flux in leads, ii) effect of snow-cover on the air–sea ice CO_2 flux over thin, young ice in the Arctic Ocean during winter and spring seasons, and iii) of the effect of the temperature difference between sea ice and atmosphere (including snow cover) on the air–sea ice CO_2 flux.

2 Materials and Methods

2.1 Study area

This study was performed during N-ICE2015 campaign with R/V Lance in the pack ice north of Svalbard from January to June 2015 (Granskog et al., 2016). Air–sea ice CO_2 flux measurements were carried out from January to May 2015 during the drift of floes 1, 2, and 3 of the N-ICE2015 campaign (Figures 1 and 2, Table 1). The ice pack was a mixture of young ice, first-year ice and second-year ice (Granskog et al., 2017), and both the first- and second-year ice had a thick snow cover (Merkouriadi et al., 2017; Rösel et al., 2018). Air–sea ice CO_2 flux measurements were made over young ice (YI stations), first-year ice (FI stations), and old ice (multi-year ice) (OI station). In the N-ICE2015 study region, the modal ice thickness was about 1.3–1.5 m and the modal snow thickness was about 0.5 m (Rösel et al., 2018). Formation of leads and their rapid refreezing provided us the opportunity to examine air–sea ice CO_2 fluxes over thin sea ice, occasionally covered with frost flowers at station YI1 (Figure 2 and Table 1). Air temperature and wind speed were measured at a 10 m weather mast on the ice floe installed about 400 m away from R/V Lance (Cohen et al., 2017).

2.2 CO_2 flux measurements

The air–sea ice CO_2 flux was measured with LI-COR 8100-104 chambers connected to a LI-8100A soil CO_2 flux system (LI-COR Inc., USA) (Figure 2). This enclosed chamber method has been widely applied over snow and sea ice (e.g., Schindlbacher et

al., 2007, Geilfus et al., 2015). Two chambers were connected in a closed loop to the infrared gas analyzer (LI-8100A, LI-COR Inc., USA) to measure CO_2 concentration through the multiplexer (LI-8150, LI-COR Inc., USA) with an air pump rate at 3 L min^{-1}. Power was supplied by a car battery (8012-254, Optima Batteries Inc., USA). Four CO_2 standards (324–406 ppmv) traceable to the WMO scale (Inoue and Ishii, 2005) were prepared to calibrate the CO_2 gas analyzer prior to the observations. CO_2 flux was measured in the morning or in the afternoon during low-wind conditions (Table 2), to minimize the effect of wind on the flux (Bain et al., 2005).

One chamber was installed over undisturbed snow or frost flowers on the ice surface. The chamber collar was inserted 5 cm into the snow and 1 cm into ice at the frost flower site to avoid air leaks between the inside and outside of the chamber. The second chamber was installed on bulk sea ice after removing the snow or frost flowers. Flux measurements were begun immediately in order to minimize the changes of the ice surface condition. In order to evaluate the effect of removing snow on the ice surface temperature, temperature was monitored during CO_2 flux measurements at station FI6. A temperature sensor (RTR 52, T & D Corp., Japan) was installed in the top of the ice (1 cm) surface after snow removal. During the first CO_2 flux measurements (about 30 minutes), the ice surface temperature was stable at –5.8°C, suggesting that the effect of removing snow on the variation of sea ice surface temperature was negligible within 30 minutes. The ice surface temperature decreased from –5.8°C to –8.0°C at 200 minutes after removal of snow. Therefore, in this paper, the data of the initial 30 minutes of CO_2 flux measurement after removal of snow or frost flowers was used. The chamber was closed for 20 minutes in a sequence. The 20-minute time period was used because CO_2 fluxes over sea ice are much smaller than over land. The CO_2 concentrations within the chamber were monitored to ensure that they changed linearly throughout the measurement period (example given in Figure 3). The CO_2 flux (mmol C m^{-2} day^{-1}) (positive value indicates CO_2 being released from ice surface to air) was calculated based on the changes of the CO_2 concentration within the headspace of the chamber with LI-COR software (Model: LI8100PC Client v.3.0.1.). The mean coefficient of variation for CO_2 flux measurements was less than 3.0% for CO_2 flux values larger than ±0.1 mmol C m^{-2} day^{-1}. For CO_2 flux values smaller than ±0.1 mmol C m^{-2} day^{-1}, the

mean coefficient of variation for CO_2 flux measurements was higher than 3.0%, suggesting that the detection limit of this system is about 0.1 mmol C m^{-2} day^{-1}.

In this paper, we express the CO_2 flux measured over the snow and frost flowers as F_{snow} and F_{ff}, respectively. The flux measured directly over the sea ice surface either on snow-free ice or after removal of snow and frost flowers as F_{ice}. F_{snow} and F_{ff} are the natural flux (snow and frost flowers are part of the natural system), and F_{ice} is the potential flux in cases when snow or frost flowers are removed. While removal of snow and frost flowers is an artificial situation, comparisons between F_{ice} and F_{snow} or F_{ff} provide information about the effect of snow and frost flowers on the CO_2 flux. Therefore, in this study, we examine both situations for CO_2 flux.

2.3 Sampling of snow, frost flowers, brine, and sea ice

For salinity measurements, separate samples were taken for snow only, snow and frost flowers, and sea ice surface scrapes. The samples were taken using a plastic shovel, placed into plastic bags and stored in an insulated box for transport to the ship-lab for further processing. Samples were melted slowly (2–3 days) in the dark at +4°C. The temperature of the snow and frost flower samples were measured during CO_2 flux measurements (approximately 60 minutes after the onset of the CO_2 flux measurement) using a needle-type temperature sensor (Testo 110 NTC, Brandt Instruments, Inc., USA). The accuracy of this sensor is ±0.2°C. Snow density was obtained using a fixed volume sampler (Climate Engineering, Japan) and weight measurement. The depth of the snow pack and frost flowers was also recorded using a ruler.

Brine was also collected at stations FI3–6 for salinity, dissolved inorganic carbon (DIC) and total alkalinity (TA) measurements. Brine was collected from sackholes as described in Gleitz et al. (1995). The sackholes were drilled using a 9 cm diameter ice corer (Mark II coring system, Kovacs Enterprises, Inc., USA) to a depth of 30 cm. The sackholes were then covered with a lid of 5 cm-thick urethane to reduce heat and gas transfer between brine and atmosphere. When brine accumulated at the bottom of the

sackholes (approximately 15 minutes), it was collected with a plastic syringe (AS ONE Corporation, Japan) and kept in 500 mL unbreakable plastic bottles (I-Boy, AS ONE Corporation, Japan) in order to facilitate safe transport to the sampling sites in cold and harsh conditions. The brine bottles were filled without head-space and immediately stored in an insulated box to prevent freezing. Immediately after return to the ship, the brine samples were transferred to 250 mL borosilicate bottles (DURAN Group GmbH, Germany) for DIC and TA measurements using tubing to prevent contact with air. The samples were preserved with saturated mercuric chloride ($HgCl_2$, 60 µL for a 250 mL sample) and stored in the dark at +10°C until analyses was performed at the Institute of Marine Research, Norway.

Sea ice was collected by the same ice corer as described for brine collection and at the same location as snow and frost flowers were collected. Sea ice temperature was measured by the same sensor as described for snow. For the ice cores, the temperature sensor was inserted in small holes drilled into the core. The core was then cut with a stainless steel saw into 10 cm sections and stored in plastic bags for subsequent salinity measurements. The ice core sections were kept at +4°C and melted in the dark prior to measurement.

2.4 Sample analysis

Salinities for melted snow, frost flowers, sea ice, and brine were measured with a conductivity sensor (Cond 315i, WTW GmbH, Germany). For calibration of salinity measurement, a Guildline PORTASAL salinometer Model 8410A, standardized by International Association for the Physical Sciences of the Oceans (IAPSO) standard seawater (Ocean Scientific International Ltd, UK) was used. The accuracy of this sensor was ±0.003.

Analytical methods for DIC and TA determination are fully described in Dickson et al. (2007). DIC in brine was determined using gas extraction of acidified sample followed by coulometric titration and photometric detection using a Versatile INstrument for the

Determination of Total inorganic carbon and titration Alkalinity (VINDTA 3C, Germany). TA of brine was determined by potentiometric titration of 40 mL sample in open cell with 0.05 N hydrochloric acid using a Titrino system (Metrohm, Switzerland). The average standard deviation for DIC and TA, determined from replicate sample analyses from one sample, was within ±2 μmol kg^{-1} for both DIC and TA. The accuracy of the DIC and TA measurements were ±2 μmol kg^{-1} for both DIC and TA, as estimated using Certified Reference Materials (CRM, provided by A. G. Dickson, Scripps Institution of Oceanography, USA). The pCO_2 of brine ($pCO_{2\,b}$) was derived from in situ temperature, salinity, DIC and TA of brine using the carbonate speciation program CO2SYS (Pierrot et al., 2006). The calculated $pCO_{2\,b}$ values (Table 2) varied within 1.7% when DIC and TA values were changed within the standard deviation (±2 μmol kg^{-1}). We used the carbonate dissociation constants (K_1 and K_2) of Mehrbach et al. (1973) as refit by Dickson and Millero (1987), and the KSO_4 determined by Dickson (1990). The conditional stability constants used to derive pCO_2 are only valid for temperatures above 0 °C and salinities between 5 and 50. Studies in spring ice indicated that seawater thermodynamic relationships may be acceptable in warm and low-salinity sea ice (Delille et al., 2007). In sea ice brines at even moderate brine salinities of 80, Brown et al. (2014) found that measured and calculated values of the CO_2 system parameters can differ by as much as 40%. On the other hand, because the CO_2 system parameters are much more variable in sea ice than in seawater, sea ice measurements demand less precision than those in seawater. Fransson et al. (2015) performed one of the few detailed analyses of the internal consistency using four sets of dissociation constants and found that the deviation between measured and calculated DIC varied between ±6 and ±11 μmol kg^{-1}, respectively. This error in calculated DIC was considered insignificant in relation to the natural variability in sea ice.

The pCO_2 of atmosphere was calculated from CO_2 concentration (ppmv) at Ny-Ålesund, Svalbard (http://www.esrl.noaa.gov/gmd/dv/iadv/) taking into account saturated water vapor and atmospheric pressure during sampling day.

The water equivalent was computed for snow by multiplying snow thickness by snow density (Jonas et al., 2009). Brine volume of sea ice was calculated from the

294 temperature and salinity of sea ice according to Cox and Weeks (1983) and Petrich and
295 Eicken (2010).
296
297
298 **3 Results**
299
300 **3.1 Air temperature**
301
302 Air temperature is shown in Figure 4. During the study period, the air temperature
303 varied considerably from a low of –41.3°C (30 January) to a high of +1.7°C (15 June)
304 (Hudson et al., 2015). Even in wintertime (from January to March), rapid increases of
305 air temperature from less than –30°C up to –0.2°C (e.g., 18 February), were observed.
306 In springtime (from April to June), the air temperature increased continuously, and from
307 1 June, air temperatures were near 0°C, although rapid increases (and subsequent
308 decreases) of air temperature to near 0°C were observed on two occasions in mid-May
309 (Cohen et al., 2017).
310
311
312 **3.2 Characteristics of snow, sea ice, and frost flowers**
313
314 The snow and ice thickness at the observation sites ranged between 0.0 and 60.0 cm and
315 between 15.0 and >200 cm, respectively (Table 1). The thin snow and ice represent
316 newly formed ice in leads at station YI1. The thickness of the frost flowers ranged from
317 1.0 to 2.5 cm.
318
319 Figure 5 shows vertical profiles of snow and ice temperature and salinity in the top 20
320 cm of ice. Temperatures within the snowpack depended on the air temperature at the
321 time of observation. However, the bottom of the snow and the surface of the sea ice
322 were relatively warm (T>–7.5°C), except for the frost flower station YI1 and the multi-
323 year ice station OI1 (Figure 5a and Table 2). High salinities (S>18.6) characterized the
324 bottom of the snow and the surface of the sea ice, except for the multi-year ice station
325 OI1 (Figure 5b). At the multi-year ice station OI1, salinity was zero through the snow

and top of sea ice. Salinity of frost flowers was up to 92.8 for the thin ice station YI1 (Figure 5b). Snow density and water equivalent ranged from 268 to 400 kg m^{-3} and 11 to 180 kg m^{-2}, respectively (Table 2).

3.3 Physical and chemical properties of brine

The brine volume fraction, temperature, salinity, DIC, TA, and calculated pCO_2 are summarized in Table 2. Brine volume fraction in the top 20 cm of ice was between 9 to 17%, except for the value of 0% at the multi-year ice station OI1 (Table 2). Brine temperatures and salinity ranged from −5.3 to −3.3°C and 51.8 to 86.6, respectively. DIC and TA of brine ranged from 3261 to 4841 µmol kg^{-1} and 3518 to 5539 µmol kg^{-1}, respectively. The pCO_2 of brine ($pCO_{2\,b}$) (334−693 µatm) was generally higher than that of atmosphere ($pCO_{2\,a}$) (401 ± 7 µatm), except for station FI4.

3.4 CO_2 flux

Table 3 summarizes the CO_2 flux measurements for each surface condition. For undisturbed natural surface conditions, i.e. measurements directly on the snow surface (F_{snow}) or the frost flowers (F_{ff}) on young ice, the mean CO_2 flux was +0.2 ± 0.2 mmol C m^{-2} day^{-1} for F_{snow} and +1.0 ± 0.6 mmol C m^{-2} day^{-1} for F_{ff}. The potential flux in cases when snow or frost flowers had been removed (F_{ice}) was +2.5 ± 4.3 mmol C m^{-2} day^{-1}. The air–sea ice CO_2 fluxes measured over the ice surface (F_{ice}) increased with increasing differences in pCO_2 between brine and atmosphere ($\Delta pCO_{2\,b-a}$) with significant correlation ($R^2 = 0.9$, $p < 0.02$), but this was not the case for F_{snow} ($R^2 = 0.0$, $p < 0.96$) (Figure 6).

4 Discussion

4.1 Effect of snow cover on the physical properties of sea ice surface

In this study, we examined CO_2 fluxes between the sea ice and atmosphere in a wide range of air temperatures and diverse snow and ice conditions (Table 2). The bottom of the snow pack and the surface of the sea ice remained relatively warm (>–7.5°C) (Figure 5a, Table 2), except for stations OI1 and YI1, even though air temperature was sometimes below –40°C (Figure 4). Relatively warm ice temperatures were likely due to the upward heat transport from the bottom of the ice and in some cases the thick insulating snow cover, except for stations OI1 and YI1 (Table 2). Therefore, snow acted as thermal insulator over sea ice, and in general the snow depths observed during N-ICE2015 point towards this being representative for first-year and second-year or older ice in the study region in winter 2015 (Rösel et al., 2018). The young and first-year ice surfaces were characterized by high salinities (Figure 5b). During sea ice formation, upward brine transport to the snow pack occurs (e.g., Toyota et al., 2011). In addition, brine within the sea ice was not completely drained as compared to that of multi-year ice. Furthermore, formation of frost flowers and subsequent wicking up of surface brine into the frost flowers also provides high salinity at the surface of sea ice (Kaleschke et al., 2004; Geilfus et al., 2013; Barber et al., 2014; Fransson et al., 2015) as observed in this study (S>92) (Figure 5b). Snowfall over the frost flowers would have preserved the high salinity at the bottom of snow pack and top of sea ice for young and first-year ice.

As a result of the combination of the relatively high temperature and high salinity at the top of sea ice, brine volume fractions in the upper parts of the sea ice were high, up to 17% (Table 2). It has been shown that ice permeability increases by an order of magnitude when brine volume fraction is greater than 5% as compared to when the brine volume fraction is less than 5% (Golden et al., 1998; Pringle et al., 2009; Zhou et al., 2013). A brine volume fraction of 5% would correspond to a temperature of –5°C for a bulk ice salinity of 5 – the so called “law of fives” (Golden et al., 1998). Because sea ice temperatures are low, thereby reducing the permeability in winter season, air–sea ice CO_2 flux is generally at its minimum in the winter (e.g., Delille et al., 2014). However, in our study, the brine volume fractions were generally >9%, except for station OI1 with fresh ice at the surface, providing conditions for active gas exchange

within sea ice and between sea ice and atmosphere. This situation was likely made possible due to the thick snow cover and relatively thin and young sea ice.

4.2 CO_2 fluxes over different sea-ice surface types

The CO_2 flux measurements over different surface conditions indicate that the snow cover over sea ice affects the magnitude of air–sea ice CO_2 flux, especially for stations FI5 and FI6 (Table 3). For undisturbed natural surface conditions, the CO_2 flux measured directly over snow-covered first-year ice and young ice with frost flowers (F_{snow} and F_{ff}) was lower in magnitude than that for potential flux obtained directly over the ice surface after removing snow (F_{ice}) for stations FI5, FI6, and YI1.

F_{ff} indicates that the frost flower surface on young thin ice is a CO_2 source to the atmosphere and F_{ff} was higher than F_{snow}, except for station FI1. This finding was consistent with the previous studies (Geilfus et al., 2013; Barber et al., 2014; Fransson et al., 2015). At multi-year ice station OI1, neither snow or ice surface acted as a CO_2 source/sink. The surface of multi-year ice did not contain any brine (Figure 5b and Table 2), and the top of the ice was clear, colorless and very hard, suggesting superimposed formation at the top of sea ice. This situation would be similar as for freshwater-ice and superimposed-ice as these non-porous media block gas exchange effectively at the sea ice surface (Delille et al., 2014). Snow-ice and superimposed-ice were frequently found in second-year ice cores during N-ICE2015 (Granskog et al., 2017), so the 'blocking' of gas exchange in second-year and multi-year ice may be a widespread process in the Arctic.

The magnitude of positive F_{snow} is less than F_{ice} for stations FI5 and FI6 (Table 3) indicating that the potential CO_2 flux from sea ice decreased due to the presence of snow. Previous studies have shown that snow accumulation over sea ice effectively impedes CO_2 exchange (Nomura et al., 2013; Brown et al., 2015). Nomura et al. (2013) reported that 50–90% of the potential CO_2 flux was reduced due to the presence of snow/superimposed-ice at the water equivalent of 57–400 kg m^{-2}, indicating that the

422 snow properties are an important factor that controls the CO_2 exchange through a
423 snowpack. Comparisons between stations FI5 and FI6 for F_{snow}/F_{ice} ratio (0.23 for FI5
424 and 0.02 for FI6) and water equivalent (11 kg m^{-2} for FI5 and 127 kg m^{-2} for FI6)
425 indicate that the potential CO_2 flux is reduced (80% for FI5 and 98% for FI6 of the
426 potential CO_2 flux) with increasing water equivalent. Although the magnitude of the
427 potential CO_2 flux through the sea ice surface decreased by the presence of snow for
428 stations FI5 and FI6 (Table 3), the snow surface still presents a CO_2 source to the
429 atmosphere for low snow density and shallow depth conditions (e.g., +0.6 mmol C m^{-2}
430 day^{-1} for FI5).
431
432 For F_{ice}, there were negative CO_2 fluxes at stations FI3 and FI4 (–0.6 mmol C m^{-2} day^{-1}
433 for FI3 and –0.8 mmol C m^{-2} day^{-1} for FI4) (Table 3). These fluxes corresponded to low
434 or negative $\Delta pCO_{2\ b-a}$ (Table 2 and Figure 6). Negative CO_2 fluxes should correspond to
435 negative $\Delta pCO_{2\ b-a}$. Therefore, the uncertainty for the calculation of carbonate
436 chemistry may be one reason for the discrepancy in pCO_2 calculation at station FI3
437 (Brown et al., 2014).
438
439
440 **4.3 Comparison to earlier studies on sea-ice to air CO_2 flux**
441
442 The CO_2 fluxes measured over the undisturbed natural surface conditions (F_{snow} and F_{ff})
443 in this study ranged from +0.1 to +1.6 mmol C m^{-2} day^{-1} (Table 3), which are at the
444 lower end of the reported range based on the chamber method and eddy covariance
445 method for natural and artificial sea ice (–259.2 to +74.3 mmol C m^{-2} day^{-1})
446 (Zemmelink et al., 2006; Nomura et al., 2006, 2010a, 2010b, 2013; Miller et al., 2011;
447 Papakyriakou and Miller, 2011; Geilfus et al., 2012, 2013; 2014; Barber et al., 2014;
448 Delille et al., 2014; Sørensen et al., 2014; Brown et al., 2015; Kotovitch et al., 2016).
449 Direct comparison to these previous studies is complicated because CO_2 flux
450 measurements with both chamber and eddy covariance techniques were used during
451 different conditions and ice surface characteristics. In addition, discrepancies between
452 chamber and eddy covariance measurements of air-ice CO_2 fluxes have been repeatedly
453 observed. The footprint size of CO_2 exchange measured with the two approaches

(Zemmelink et al., 2006, 2008; Burba et al., 2008; Amiro, 2010; Miller et al., 2011; Papakyriakou and Miller, 2011; Sørensen et al., 2014; Miller et al., 2015) may be one reason for the large difference. The eddy covariance method reflects a flux integrated over a large area that can contain several different surface types. Therefore, eddy-covariance appears to be more useful for understanding fluxes at large spatial and temporal scales. On the other hand, the chamber method reflects the area where chamber was covered, and it is useful for understanding the relationship between fluxes and ice surface conditions on smaller scales. The different spatial scales of the two methods may be therefore one reason for the discrepancy in CO_2 flux measurements.

Comparison of the natural CO_2 flux range (+0.1 to +1.6 mmol C m^{-2} day^{-1} for F_{snow} and F_{ff}) (Table 3) with previous estimates derived from the chamber method (–5.2 to +6.7 mmol C m^{-2} day^{-1}) (Nomura et al., 2006, 2010a, 2010b, 2013; Geilfus et al., 2012, 2013; 2014; Barber et al., 2014; Delille et al., 2014; Brown et al., 2015; Kotovitch et al., 2016) (these studies include both natural and potential fluxes) shows that CO_2 fluxes during the N-ICE2015 experiment are at the lower end of positive values. However, our potential CO_2 flux (F_{ice}) was a larger CO_2 source (up to +11.8 mmol C m^{-2} day^{-1}) than reported in previous studies (+6.7 mmol C m^{-2} day^{-1}). In our study, the maximum potential flux (+11.8 mmol C m^{-2} day^{-1}) was obtained for F_{ice} at station FI6 (Table 3). In this situation, $\Delta pCO_{2\ b-a}$ (293 µatm) was the highest (Table 2 and Figure 6), and it is reasonable to consider this as the highest magnitude of positive CO_2 flux within our study. However, a previous study by closed chamber method showed that even for a similar $\Delta pCO_{2\ b-a}$ (297 µatm) and brine volume fraction (10–15%), the CO_2 flux was +0.7 mmol C m^{-2} day^{-1} for artificial sea ice with no snow in the tank experiment (Nomura et al., 2006).

The CO_2 flux between the sea ice and overlying air can be expressed by the following equation,

$$F_{CO2} = r_b\ k\ \alpha\ \Delta pCO_{2\ b-a},$$

where r_b is the ratio of surface of the brine channel to sea ice surface, and we assume that the value of r_b is equal to brine volume fraction, k is the gas transfer velocity, α is the solubility of CO_2 (Weiss, 1974), and $\Delta pCO_{2\ b-a}$ is the difference in pCO_2 between brine and atmosphere. The equation is based on the fact that CO_2 transfer between seawater and air is controlled by processes in the near-surface water (Liss, 1973). The gas transfer velocity (k) calculated from F, r_b, α and $\Delta pCO_{2\ b-a}$ was 5.12 m day^{-1} for F_{ice} at station FI6 and 0.29 m day^{-1} for the tank experiment examined in Nomura et al. (2006). This result clearly indicates that the gas transfer velocity for F_{ice} at station FI6 is higher than that of tank experiment examined in Nomura et al. (2006) even with very similar $\Delta pCO_{2\ b-a}$ and brine volume fraction.

Here, we surmise that the gas transfer velocity and thereby CO_2 flux is greatly enhanced by the temperature difference between sea ice surface and atmosphere. Previous studies indicate that there is an unstable air density gradient in a dry snowpack due to basal heating and the strong temperature difference develops between bottom and top of snow (e.g., Powers et al., 1985; Severinghaus et al., 2010), which enhances the flow of air through the snowpack. We propose that the mixing and transport of gas within the snowpack could also occur over sea ice. Because temperatures at the bottom of snow and the top of sea ice were relatively warm due to a thick insulating snow over sea ice, there was a strong temperature difference between sea ice surface and atmosphere when air temperature was low (Figure 5a and Table 2). For station FI6, the temperature difference between the sea ice surface and atmosphere was 20.2°C after snow removal. On the other hand, in the tank experiment by Nomura et al. (2006), the temperature difference between sea ice surface (top 1.5 cm) and air in the headspace was only 4.5°C.

Figure 6 shows the relationship between mean air–sea ice CO_2 fluxes and temperature difference between ice and atmosphere. The strong dependence of CO_2 flux with temperature difference (T_{ice}–T_a) was observed, especially for F_{ff} and F_{ice} ($R^2 > 0.7$, $p < 0.01$, linear fitting) (Figure 6). Due to the high brine volume fractions (Table 2), the sea ice surface had enough permeability for gas exchange. In addition, ice temperatures were similar for young and first-year ice (Table 2), indicating that pCO_2 at the top of the

sea ice and CO_2 flux would be of similar order of magnitude if thermodynamic processes dominated. Therefore, our results suggest that the CO_2 fluxes even over the frost flowers as a natural condition, would be enhanced by the upward transport of air containing high CO_2 from the surface of sea ice to the atmosphere due to the strong temperature difference between sea ice surface and atmosphere. Although the presence of snow on sea ice has potential to produce a larger temperature difference between sea ice surface and atmosphere and promote the upward transport, the magnitude of the CO_2 flux decreased due to the presence of snow. However, for young sea ice with frost flowers (e.g., station YI1), ice surface temperature was warm (Table 2), suggesting that CO_2 flux would be enhanced by the large temperature difference between sea ice surface and atmosphere.

5 Conclusions

We measured CO_2 fluxes along with sea ice and snow physical and chemical properties over first-year and young sea ice north of Svalbard in the Arctic pack ice. Our results suggest that young thin snow-free ice, with or without frost flowers, is a source of atmospheric CO_2 due to the high pCO_2 and salinity and relatively high sea ice temperature. Although the potential CO_2 flux from the sea ice surface decreased due to the presence of snow, the snow surface still presents a modest CO_2 source to the atmosphere for low snow density and shallow depth situations. The highest ice-to-air fluxes were observed over thin young sea ice formed in leads. During N-ICE2015 the ice pack was dynamic, and formation of open water was associated with storms, where new ice was formed. The subsequent ice growth in these leads is especially important for the ice-to-air CO_2 fluxes in winter since the flux from young ice is an order of magnitude larger than from snow-covered first-year and older ice.

6 Data availability

Data used in this paper will be available at Norwegian Polar Data Centre (data.npolar.no).

7 Acknowledgments

We would like to express heartfelt thanks to the crew of R/V Lance and all members of the N-ICE2015 expedition for their support in conducting the field work. This work was supported by the Japan Society for the Promotion of Science (#15K16135, #24-4175), Research Council of Norway (KLIMAFORSK programme, grant 240639), the Centre of Ice, Climate and Ecosystems (ICE) at the Norwegian Polar Institute through the N-ICE project, the Ministry of Climate and Environment and the Ministry of Foreign Affairs of Norway and the Grant for Joint Research Program of the Institute of Low Temperature Science, Hokkaido University. AF, MC and MAG were supported by the flagship research program "Ocean acidification and ecosystem effects in Northern waters" within the FRAM-High North Research Centre for Climate and the Environment. BD is a research associate of the F.R.S-FNRS.

Reference list

Amiro, B.: Estimating annual carbon dioxide eddy fluxes using open-path analysers for cold forest sites. Agr. Forest Meteorol., 150, 15, 1366–1372. 2010.

Bain, W. G., Hutyra, L., Patterson, D. C., Bright, A. V.,Daube, B. C. Munger, J. W., Wofsy, S. C.: Wind-induced error in the measurement of soil respiration using closed dynamic chambers. Agricul. Forest Meteo., 131, 3–4, 225–232, 2005.

579 Barber, D. G., Ehn, J. K., Pućko, M., Rysgaard, S., Deming, J. W. and co-authors: Frost
580 flowers on young Arctic sea ice: The climatic, chemical and microbial significance of
581 an emerging ice type. J Geophys. Res.-Atmos. doi: 10.1002/2014JD021736. 2014.
582
583 Brown, K. A, Miller, L. A., Davelaar, M., Francois, R., and Tortell P. D.: Over-
584 determination of the carbonate system in natural sea ice brine and assessment of
585 carbonic acid dissociation constants under low temperature, high salinity conditions.
586 Mar. Chem 165: 36–45. doi: 10.1016/j.marchem.2014.07.005. 2014.
587
588 Brown, K. A., Miller, L.A., Mundy, C. J., Papakyriakou, T., Francois, R., and co-
589 authors: Inorganic carbon system dynamics in landfast Arctic sea ice during the early-
590 melt period. J. Geophys. Res. Oceans, 120, 3542–3566.
591 http://dx.doi.org/10.1002/2014JC010620. 2015.
592
593 Burba, G., McDermitt, D., Grelle, A., Anderson, D., and Xu, L.: Addressing the
594 influence of instrument surface heat exchange on the measurements of CO_2 flux from
595 open-path gas analyzers, Global Change Biol., 14, 8, 1854–1876, 2008.
596
597 Cohen, L., Hudson, S. R., Walden, V. P., Graham, R. M., and Granskog, M. A.:
598 Meteorological conditions in a thinner Arctic sea ice regime from winter through
599 summer during the Norwegian young sea ICE expedition (N-ICE2015), J. Geophys. Res.
600 Atmos., 122, 7235–7259, doi:10.1002/2016JD026034, 2017.
601
602 Cox, G. F. N., and Weeks W. F.: Equations for determining the gas and brine volumes
603 in sea-ice samples, J. Glaciol., 29, 306–316, 1983.
604
605 Delille, B., Jourdain, B., Borges, A. V., Tison, J.-L., and Delille, D.: Biogas (CO_2, O_2,
606 dimethylsulfide) dynamics in spring Antarctic fast ice, Limnol. Oceanogr., 52, 1367–
607 1379, 2007.
608

609 Delille, B., Vancoppenolle, M., Geilfus, N.-X.. Tilbrook, B. Lannuzel.D., and co-
610 authors: Southern Ocean CO_2 sink: the contribution of the sea ice, J. Geophys. Res.
611 Oceans. 119 (9), 6340–6355, 2014.
612
613 Dickson, A. G., and Millero F. J.: A comparison of the equilibrium constants for the
614 dissociation of carbonic acid in seawater media, Deep-Sea Res. 34, 1733–1743, 1987.
615
616 Dickson, A. G.: Thermodynamics of the dissociation of boric acid in synthetic seawater
617 from 273.15 to 318.15 K, Deep-Sea Res. 37, 755–766, 1990.
618
619 Dickson, A. G., Sabine, C. L., and Christian, J. R. Eds.: Guide to Best Practices for
620 Ocean CO_2 Measurements, PICES Special Publication, 3, 191 pp, 2007.
621
622 Fransson, A., Chierici, M., Miller, L. A., Carnat, G., Thomas, H., and co-authors:
623 Impact of sea ice processes on the carbonate system and ocean acidification state at the
624 ice-water interface of the Amundsen Gulf, Arctic Ocean, J. Geophys. Res., 118, 1–23,
625 doi:10.1002/2013JC009164, 2013.
626
627 Fransson, A., Chierici, M., Abrahamsson, K., Andersson, M., Granfors, A., and co-
628 authors: CO_2-system development in young sea ice and CO_2 gas exchange at the ice/air
629 interface mediated by brine and frost flowers in Kongsfjorden, Spitsbergen, Ann.
630 Glaciol., 56, 69, doi: 10.3189/2015A0G69A563, 2015.
631
632 Fransson, A., Chierici, M., Skjelvan, I., Olsen, A., Assmy, P., Peterson, A. K., Ward,
633 B.: Effects of sea-ice and biogeochemical processes and storms on under-ice water f
634 CO_2 during the winter-spring transition in the high Arctic Ocean: Implications for sea-
635 air CO_2 fluxes, J. Geophys. Res. Oceans, 122(7), 5566–5587.
636 https://doi.org/10.1002/2016JC012478. 2017.
637
638 Geilfus, N.-X., Carnat, G., Papakyriakou, T., Tison, J.-L., Else, B. and co-authors:
639 Dynamics of pCO_2 and related air–ice CO_2 fluxes in the Arctic coastal zone (Amundsen
640 Gulf, Beaufort Sea), J. Geophys. Res., 117, C00G10, doi:10.1029/2011JC007118, 2012.

Geilfus, N.-X., Carnat, G., Dieckmann, G. S., Halden, N., Nehrke, G., and co-authors:. First estimates of the contribution of $CaCO_3$ precipitation to the release of CO_2 to the atmosphere during young sea ice growth, J. Geophys. Res., 118:244–255. http://dx.doi.org/10.1029/2012JC007980, 2013.

Geilfus, N.-X., Tison, J.-L., Ackley, S. F., Galley, R. J., Rysgaard, S., and co-authors: Sea ice pCO_2 dynamics and air–ice CO_2 fluxes during the Sea Ice Mass Balance in the Antarc-tic (SIMBA) experiment – Bellingshausen Sea, Antarctica, The Cryosphere, 8, 2395–2407, doi:10.5194/tc-8-2395-2014, 2014.

Geilfus, N.-X., Galley, R. J., Crabeck, O., Papakyriakou, T., Landy, J., Tison, J.-L. and Rysgaard, S.: Inorganic carbon dynamics of melt-pond-covered first-year sea ice in the Canadian Arctic, Biogeosci., 12, 2047–2061, doi:10.5194/bg-12-2047-2015, 2015.

Gleitz, M., Vonderlo, M. R., Tomas, D. N., Dieckmann, G. S. and Millero F. J.: Comparison of summer and winter inorganic carbon, oxygen and nutrient concentrations in Antarctic sea ice brine, Mar. Chem., 51, 81–89, 1995.

Golden, K. M., Ackley, S. F. and Lytle, V. I.: The percolation phase transition in sea ice, Science, 282, 2238–2241, 1998.

Granskog, M. A., Assmy, P., Gerland, S., Spreen, G., Steen, H., and co-authors: Arctic research on thin ice: Consequences of Arctic sea ice loss, Eos Transactions AGU, 97, 22–26, doi:10.1029/2016EO044097, 2016.

Granskog, M. A., Rösel, A., Dodd, P. A., Divine, D., Gerland, S., and co-authors: Snow contribution to first-year and second-year Arctic sea ice mass balance north of Svalbard, J. Geophys. Res. Oceans, 122, 2539-2549, doi: 10.1002/2016JC012398, 2017.

Hudson, S. R., Cohen, L., and Walden, V.: N-ICE2015 surface meteorology (Data set), Norwegian Polar Institute, doi: 10.21334/npolar.2015.056a61d1, 2015.

673
674 Inoue, H. Y. and Ishii M.: Variations and trends of CO_2 in the surface seawater in the
675 Southern Ocean south of Australia between 1969 and 2002, Tellus, Ser. B, 57, 58–69,
676 2005.
677
678 Jonas, T., Marty, C., and Magnusson, J.: Estimating the snow water equivalent from
679 snow depth measurements in the Swiss Alps, J. Hydrol., 378, 161–167, 2009.
680
681 Kaleschke, L., Richter, A., Burrows, J., Afe, O., Heygster, G., and co-authors: Frost
682 flowers on sea ice as a source of sea salt and their influence on tropospheric halogen
683 chemistry, Geophys. Res. Lett., 31, L16114, doi:10.1029/2004GL020655, 2004.
684
685 Kotovitch, M., Moreau, S., Zhou, J., Vancoppenolle, M., Dieckmann, G. S., and co-
686 authors: Air–ice carbon pathways inferred from a sea ice tank experiment, Elementa:
687 Science of the Anthropocene, 4, 1, doi10.12952/journal.elementa.000112, 2016.
688
689 Lindsay, R., and Schweiger, A.: Arctic sea ice thickness loss determined using
690 subsurface, aircraft, and satellite observations, The Cryosphere, 9(1), 269–283,
691 doi:10.5194/tc-9-269-2015, 2015.
692
693 Liss, P. S.: Processes of gas exchange across an air-water interface, Deep-Sea Res. 20,
694 221–238, 1973.
695
696 Massman, W., Sommerfeld, R., Zeller, K., Hehn, T., Hudnell, L., and Rochelle, S.: CO_2
697 flux through a Wyoming seasonal snowpack: diffusional and pressure pumping effects,
698 Biogeochemistry of Seasonally Snow-Covered Catchments (Proceedings of a Boulder
699 Symposium, July 1995). IAHS Publ., 228, 71–79, 1995.
700
701 Massom, R.A., Eicken, H., Haas, C., Jeffries, M. O., Drinkwater, M. R., and other co-
702 authors: Snow on Antarctic sea ice, Reviews of Geophysics, 39, 413–445, 2001.
703

Mehrbach, C., Culberson, C. H., Hawley, J. E., and Pytkowicz P. M.: Measurement of the apparent dissociation constant of carbonic acid in seawater at atmospheric pressure, Limnol. Oceanogr., 18, 897–907, 1973.

Meier, W. N., Hovelsrud, G. K., van Oort, B. E. H., Key, J. R., Kovacs, K. M., and co-authors: Arctic sea ice in transformation: A review of recent observed changes and impacts on biology and human activity, Rev. Geophys., 52, 185–217, doi:10.1002/2013RG000431, 2014.

Miller, L. A., Papakyriakou, T. N., Collins, R. E., Deming, J. W., Ehn, J. K., and co-authors: Carbon dynamics in sea ice: A winter flux time series, J. Geophys. Res., 116, C02028, doi:10.1029/2009JC006058, 2011.

Miller, L. A., Fripiat, F., Else, B. G. T., Bowman, J. S., Brown, K. A., and co-authors:. Methods for Biogeochemical Studies of Sea Ice: The State of the Art, Caveats, and Recommendation, Elementa, 3, 000038, doi:10.12952/journal.elementa.000038, 2015.

Nomura, D., Inoue, H. Y., and Toyota, T.: The effect of sea-ice growth on air–sea CO_2 flux in a tank experiment, Tellus, Ser. B, 58, 418–426, 2006.

Nomura, D., Inoue, H. Y., Toyota, T., and Shirasawa, K.: Effects of snow, snowmelting and refreezing processes on air–sea-ice CO_2 flux, J. Glaciol., 56, 196, 262–270, 2010a.

Nomura, D., Eicken, H., Gradinger, R., and Shirasawa, K.: Rapid physically driven inversion of the air-sea ice CO_2 flux in the seasonal landfast ice off Barrow, Alaska after onset of surface melt, Cont. Shelf Res., 30, 1998–2004, 2010b.

Nomura, D., Granskog, M. A., Assmy, P., Simizu, D., and Hashida, G.: Arctic and Antarctic sea ice acts as a sink for atmospheric CO_2 during periods of snow melt and surface flooding, J. Geophys. Res. Oceans, 118, 6511–6524, 2013.

735 Merkouriadi, I., Gallet, J.-C., Graham, R. M., Liston, G. E., Polashenski, C., Rösel, A.,
736 and Gerland, S.: Winter snow conditions on Arctic sea ice north of Svalbard during the
737 Norwegian young sea ICE (N-ICE2015) expedition, J. Geophys. Res. Atmos., 122,
738 doi:10.1002/2017JD026753, 2017.
739
740 Papadimitriou, S., Kennedy, H., Norman, L., Kennedy, D. P., Dieckmann, G. S., and
741 co-authors: The effect of biological activity, $CaCO_3$ mineral dynamics, and CO_2
742 degassing in the inorganic carbon cycle in sea ice in late winter-early spring in the
743 Weddell Sea, Antarctica, J. Geophys. Res. 117, C08011, doi:10.1029/2012JC008058,
744 2012.
745
746 Papakyriakou, T., and Miller, L. A.: Springtime CO_2 exchange over seasonal sea ice in
747 the Canadian Arctic Archipelago, Ann. Glaciol., 52, 57, 215–224, 2011.
748
749 Parmentier, F. J. W., Christensen, T. R., Sørensen, L. L., Rysgaard, S., McGuire, A. D.,
750 and co-authors: The impact of lower sea-ice extent on Arctic greenhouse-gas exchange,
751 Nature Climate Change, 3, 195–202, doi:10.1038/nclimate1784, 2013.
752
753 Petrich, C. and Eicken, H.: Growth, structure and properties of sea ice, in Thomas, D. N.
754 and Dieckmann, G. S. eds., Sea Ice, 2nd ed., Oxford, Wiley-Blackwell, 23–77, 2010.
755
756 Pierrot, D., Lewis, E. and Wallace, D. W. R.: MS Excel Program Developed for CO_2
757 System Calculations, ORNL/CDIAC-105a. Carbon Dioxide Information Analysis
758 Center, Oak Ridge National Laboratory, U.S. Department of Energy, Oak Ridge,
759 Tennessee, doi: 10.3334/CDIAC/otg.CO2SYS_XLS_CDIAC105a, 2006.
760
761 Powers, D., Oneill, K., and Colbeck, S. C.: Theory of natural convection in snow, J.
762 Geophys. Res.-Atmos., 90, 10641–10649, doi:10.1029/Jd090id06p10641, 1985.
763
764 Pringle, D. J., Miner, J. E., Eicken, H., and Golden, K. M.: Pore space percolation in sea
765 ice single crystals, J. Geophys. Res., 114, C12017, doi:10.1029/2008JC005145, 2009.
766

767 Rysgaard, S., Søgaard, D. H., Cooper, M., Pucko, M., Lennert, K., and co-authors:
768 Ikaite crystal distribution in winter sea ice and implications for CO_2 system dynamics,
769 The Cryosphere, 7, 707–718, doi:10.5194/tc-7-707-2013, 2013.
770
771 Rösel, A., Itkin, P., King, J., Divine, D., Wang, C., Granskog, M. A., Krumpen, T. and
772 Gerland, S.: Thin Sea Ice, Thick Snow, and Widespread Negative Freeboard Observed
773 During N-ICE2015 North of Svalbard, J. Geophys. Res. Oceans, 123(2), 1156–1176,
774 doi:10.1002/2017JC012865, 2018.
775
776 Schindlbacher, A., Zechmeister-Boltenstern, S., Glatzel, G., and Jandl R.: Winter soil
777 respiration from an Austrian mountain forest, Agric, For. Meteorol., 146, 205–215,
778 doi:10.1016/j.agrformet.2007.06.001, 2007.
779
780 Severinghaus, J. P., Albert, M. R., Courville, Z. R., Fahnestock, M. A., Kawamura, K.,
781 and co-authors: Deep air convection in the firn at a zero-accumulation site, central
782 Antarctica, Earth Planet. Sci. Lett., 293, 359–367, doi:10.1016/J.Epsl.2010.03.003,
783 2010.
784
785 Stroeve, J. C., Serreze, M. C., Holland, M. M., Kay, J. E., Maslanik, J., and Barrett, A.
786 P.: The Arctic's rapidly shrinking sea ice cover: a research synthesis, Climatic Change,
787 110, 1005, doi:10.1007/s10584-011-0101-1, 2012.
788
789 Sørensen, L. L, Jensen, B., Glud, R. N., McGinnis, D. F., and Sejr, M. K.:
790 Parameterization of atmosphere-surface exchange of CO_2 over sea ice, The Cryosphere,
791 8: 853–866. doi:10.5194/tc-8-853-2014, 2014.
792
793 Takagi, K., Nomura, M., Ashiya, D., Takahashi, H., Sasa, K., and co-authors: Dynamic
794 carbon dioxide exchange through snowpack by wind-driven mass transfer in a conifer-
795 broadleaf mixed forest in northernmost Japan, Global Biogeochem. Cycles, 19, GB2012,
796 doi:10.1029/2004GB002272, 2005.
797

798 Toyota, T., Massom, R., Tateyama, K., Tamura, T., and Fraser, A.: Properties of snow
799 overlying the sea ice off East Antarctica in late winter 2007, Deep Sea Res. II, 58,
800 1137–1148, 2011.
801
802 Vancoppenolle, M., Meiners, K. M., Michel, C., Bopp, L., Brabant, F., and co-authors:
803 Role of sea ice in global biogeochemical cycles: emerging views and challenges, Quat.
804 Sci. Rev., 79, 207–230, 2013.
805
806 Weiss, R. F.: Carbon dioxide in water and seawater: the solubility of a non-ideal gas,
807 Mar. Chem., 2, 203–215, 1974.
808
809 Zemmelink, H. J., Delille, B., Tison, J.-L., Hintsa, E. J., Houghton, L., and co-authors:.
810 CO_2 deposition over the multi-year ice of the western Weddell Sea, Geophys. Res. Lett.,
811 33, L13606, doi:10.1029/2006GL026320, 2006.
812
813 Zemmelink, H. J., Dacey, J. W. H., Houghton, L., Hintsa. E. J., and Liss, P. S.:
814 Dimethylsulfide emissions over the multi-year ice of the western Weddell Sea, Geophys.
815 Res. Lett., 35, L06603, doi:10.1029/2007GL031847, 2008.
816
817 Zhou, J., Delille**,** B., Eicken, H., Vancoppenolle, M., Brabant, F., and co-authors:
818 Physical and biogeochemical properties in landfast sea ice (Barrow, Alaska): Insights
819 on brine and gas dynamics across seasons, J. Geophys. Res. 118, 6, 3172–3189, 2013.
820
821
822
823 **Figure captions**
824
825 Figure 1. Location map of the sampling area north of Svalbard during N-ICE2015.
826 Image of the sea ice concentrations (a) and station map (b) were derived from Special
827 Sensor Microwave Imager (SSM/I) satellite data for mean of February 2015 and from
828 Sentinel-1 (Synthetic Aperture Radar Sensor) satellite data, respectively.
829

Figure 2. Photographs of the CO_2 flux chamber system at station YI1 north of Svalbard on Friday 13 March 2015. CO_2 flux chamber was installed over the frost flowers on the new thin ice in the refreezing lead.

Figure 3. Example of the temporal variation in CO_2 concentration (ΔCO_2) in the chambers installed at station YI1 that is use to calculate the CO_2 flux. ΔCO_2 indicates the change in CO_2 concentration inside the chamber since the chamber was closed.

Figure 4. Time series of air temperature measured at the weather mast over the ice floe (10 m height) (Hudson et al., 2015). Blank period indicates no data. Colored symbols indicate the date for the chamber flux measurements. The horizontal dashed line indicates air temperature = 0°C.

Figure 5. Vertical profiles of temperature (a) and salinity (b) in snow and sea ice (top 20 cm). The horizontal line indicates snow–ice interface. Shaded area indicates sea ice. The triangle in (a) indicates the air temperature for each station. For stations FI7 and YI2 and 3, we have no salinity data.

Figure 6. Relationships between mean air–sea ice CO_2 fluxes and temperature difference (T_{ice}–T_a) between ice (top 20 cm) (T_{ice}) and atmosphere (T_a) (circle) for F_{snow} (blue), F_{ff} (black) and F_{ice} (red) for young and first-year sea ice. Relationships between mean air–sea ice CO_2 fluxes and the difference of pCO_2 ($\Delta pCO_{2\ b–a}$) between brine ($pCO_{2\ b}$) and atmosphere ($pCO_{2\ a}$) (cross) for F_{snow} (blue) and F_{ice} (red).

Table captions

Table 1. Station, date for CO_2 flux measurement, position, floe number, surface condition, ice type and thickness of snow, frost flowers, and sea ice.

a. Sea ice coring and snow sampling was conducted on 5 March 2015.

862 b. Sea ice coring and snow sampling was conducted on 10 March 2015.
863
864
865 Table 2. Station, snow density and water equivalent, brine volume fraction, and
866 temperature for sea ice (top 20 cm), brine temperature, salinity, DIC, TA, pCO_2 ($pCO_{2\ b}$),
867 and atmospheric temperature, wind speed, pCO_2 ($pCO_{2\ a}$)[a] and $\Delta pCO_{2\ b-a}$.
868
869 a. $pCO_{2\ a}$ (µatm) was calculated from CO_2 concentration (ppmv) at Ny-Ålesund,
870 Svalbard (http://www.esrl.noaa.gov/gmd/dv/iadv/) taking into account saturated water
871 vapor and atmospheric pressure during sampling day.
872
873 b. Mean values for snow column.
874
875 c. "−" indicates no data. Due to logistical constraints, data of snow, sea ice, and brine
876 were not obtained.
877
878
879 Table 3. CO_2 flux measured over the snow (F_{snow}), frost flowers (F_{ff}), and ice surface
880 (F_{ice}). Values measured directly over undisturbed surfaces (either with frost flowers or
881 on snow surface) at a given station are indicated in bold.
882
883 a. Data of first CO_2 flux measurement after removal of snow or frost flowers.
884
885 b. "−" indicates no data.
886
887 c. Number of measurements in bracket.
888
889 d. Data from station OI1 was not included.

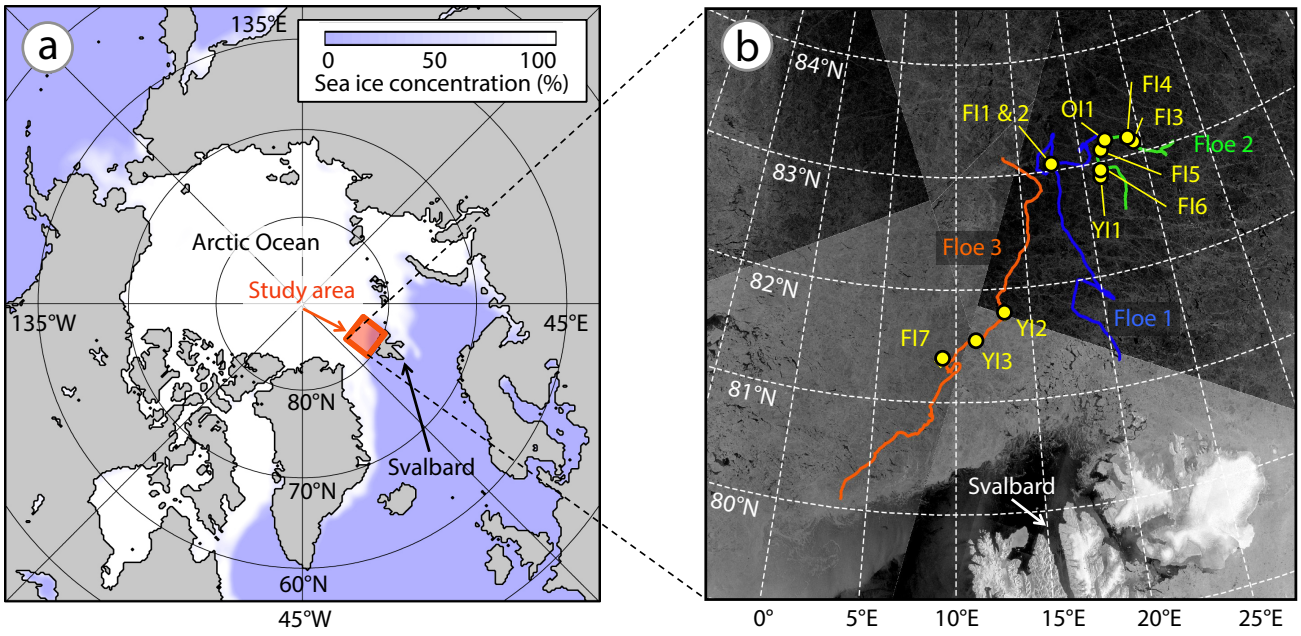

Nomura et al., Figure 1 (Double column size)

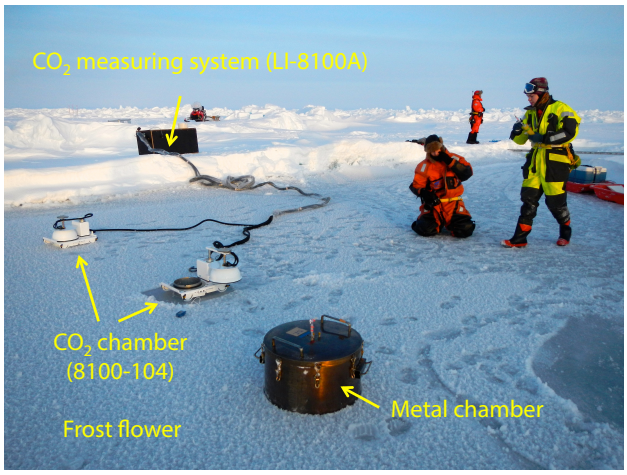

Nomura et al., Figure 2 (Single column size)

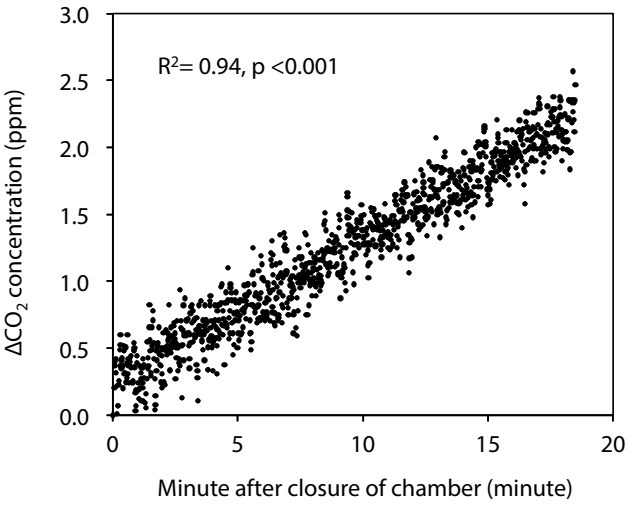

Nomura et al., Figure 3 (Single column size)

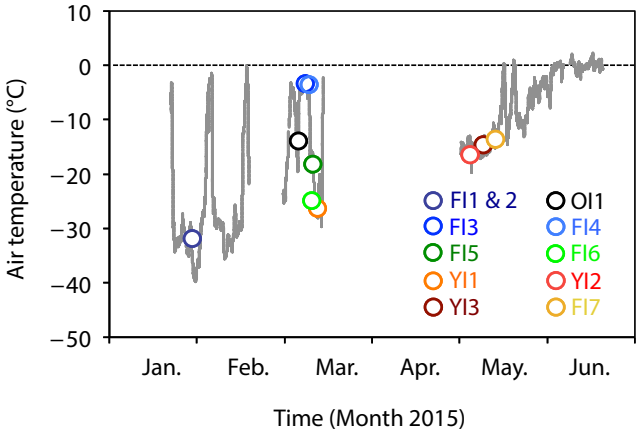

Nomura et al., Figure 4 (Single column size)

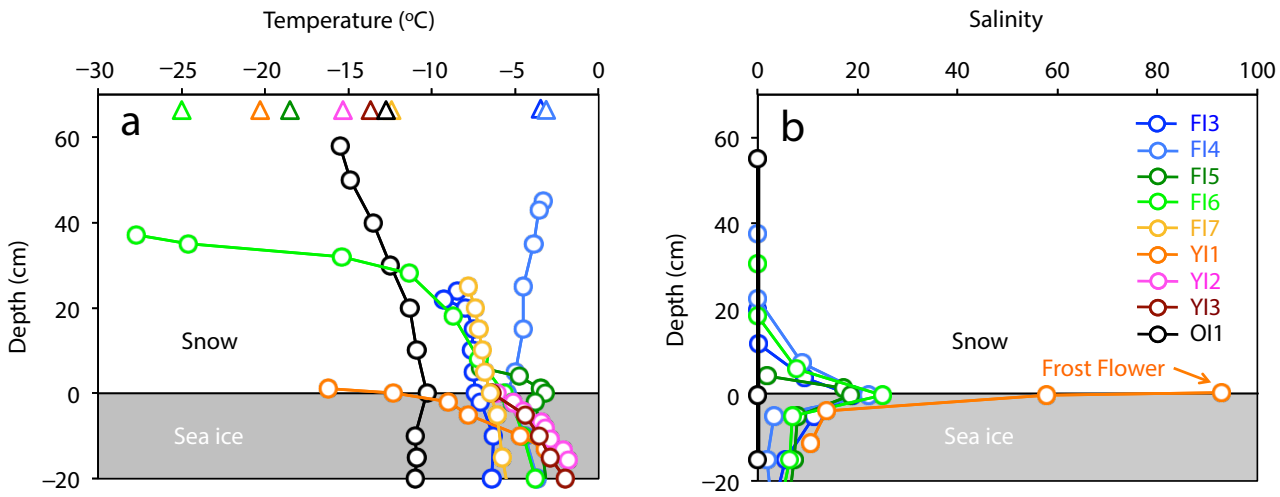

Nomura et al., Figure 5 (Double column size)

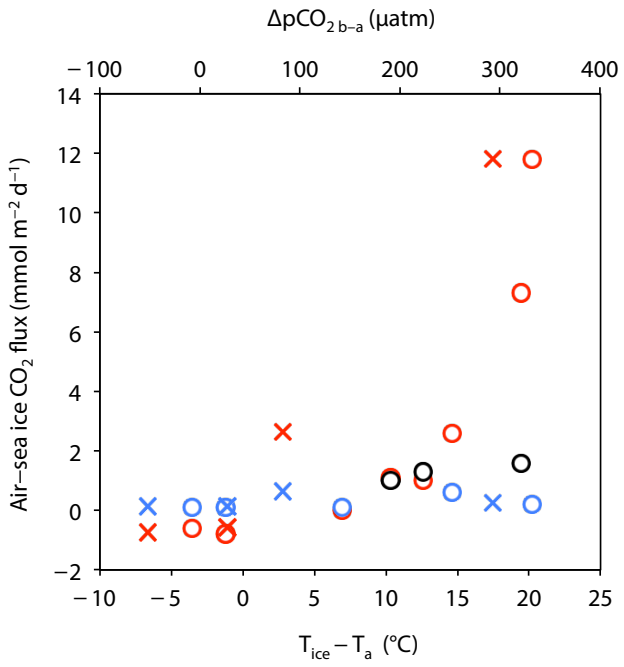

Nomura et al., Figure 6 (Single column size)

Table 1. Station, position, date for CO_2 flux measurement, floe number, surface condition, ice type and thickness of snow, frost flower, and sea ice.

Station	Position	Date of 2015	Floe number	Surface condition	Ice type[c]	Thickness (cm)		
						Snow	Frost flower	Sea ice
FI1	83º03.77N, 17º34.94E	28 January	1	Frost flower	First-year ice	0.0	1.0	37.0
FI2	83º03.77N, 17º34.94E	28 January	1	Snow	First-year ice	8.0	No	35.0
FI3	83º08.00N, 24º09.02E	5 and 8 March[a]	2	Snow	First-year ice	29.0	No	98.0
FI4	83º10.56N, 22º09.42E	9 March	2	Snow	First-year ice	36.0	No	92.0
FI5	83º06.02N, 21º38.29E	10 and 11 March[b]	2	Snow	First-year ice	3.0	No	48.0
FI6	82º55.36N, 21º25.92E	12 March	2	Snow	First-year ice	37.0	No	69.0
FI7	81º22.18N, 08º59.93E	13 May	3	Snow	First-year ice	26.5	No	127.0
YI1	82º52.52N, 21º16.54E	13 March	2	Frost flower	Young ice	0.0	1.0	15.0
YI2	81º46.53N, 13º16.00E	5 May	3	Snow and frost flower mixed	Young ice	2.5	2.5	17.5
YI3	81º32.45N, 11º17.20E	9 May	3	Snow and frost flower mixed	Young ice	2.0	2.0	22.0
OI1	83º07.18N, 24º25.59E	6 March	2	Snow	Old ice (multi-year ice)	60.0	No	>200

a. Sea ice coring, brine and snow sampling was conducted on 5 March 2015.

b. Sea ice coring, brine and snow sampling was conducted on 10 March 2015.

c. Ice type was categorized based on WMO (1970).

Table 2. Station, snow density and water equivalent, brine volume fraction and temperature for sea ice (top 20 cm), brine temperature, salinity, DIC, TA, pCO_2 ($pCO_{2\,b}$) and atmospheric temperature, wind speed, pCO_2 ($pCO_{2\,a}$)[a] and $\Delta pCO_{2\,b-a}$.

Station	Snow		Sea ice (top 20 cm)		Brine					Atmosphere			
	Density[b] ($kg\ m^{-3}$)	Water equivalent ($kg\ m^{-2}$)	Brine volume fraction (%)	Temperature (ºC) (range)	Temperature (ºC)	Salinity	DIC ($\mu mol\ kg^{-1}$)	TA ($\mu mol\ kg^{-1}$)	$pCO_{2\,b}$ (µatm)	Temperature (ºC)	Wind speed ($m\ second^{-1}$)	$pCO_{2\,a}$ (µatm)	$\Delta pCO_{2\,b-a}$ (µatm)
FI1	–[c]	–[c]	–[c]	–[c]	–[c]	–[c]	–[c]	–[c]	–[c]	−31.6	4.0	405	–[c]
FI2	–[c]	–[c]	–[c]	–[c]	–[c]	–[c]	–[c]	–[c]	–[c]	−31.6	4.0	405	–[c]
FI3	399	104	9	−6.8 (−7.4 to −6.3)	−5.2	84.8	4628	5539	427	−3.3	9.0	400	27
FI4	400	180	9	−4.7 (−5.5 to −3.7)	−5.3	86.6	4433	5490	334	−3.5	6.2	386	−52
FI5	268	11	17	−3.5 (−3.8 to −3.1)	−3.3	51.8	3261	3518	472	−18.1	6.8	389	83
FI6	343	127	13	−4.8 (−5.7 to −3.8)	−4.8	84.0	4841	5493	693	−25.0	3.6	400	293
FI7	–[c]	–[c]	–[c]	−6.1 (−6.1 to −5.8)	–[c]	–[c]	–[c]	–[c]	–[c]	−13.0	5.8	405	–[c]
YI1	–[c]	–[c]	17	−6.6 (−12.3 to −2.6)	–[c]	–[c]	–[c]	–[c]	–[c]	−26.0	2.6	402	–[c]
YI2	–[c]	–[c]	–[c]	−3.6 (−5.1 to −1.8)	–[c]	–[c]	–[c]	–[c]	–[c]	−16.2	4.5	407	–[c]
YI3	–[c]	–[c]	–[c]	−3.9 (−6.4 to −2.0)	–[c]	–[c]	–[c]	–[c]	–[c]	−14.2	6.7	410	–[c]
OI1	–[c]	–[c]	0	−10.8 (−11.0 to −10.9)	–[c]	–[c]	–[c]	–[c]	–[c]	−13.5	4.7	397	–[c]

a. $pCO_{2\,a}$ (µatm) was calculated from CO_2 concentration (ppmv) at Ny-Ålesund, Svalbard (http://www.esrl.noaa.gov/gmd/dv/iadv/) taking into account the saturated water vapor and atmospheric pressures at sampling day.

b. Mean values for column.

c. "–" indicates no data. Due to logistical constraints, data of snow, sea ice, and brine were not obtained.

Table 3. CO_2 flux measured over the snow (F_{snow}), frost flowers (F_{ff}) and ice surface (F_{ice}).

Station	CO_2 flux (mmol C m^{-2} day^{-1})		
	Natural flux (mean ± 1SD)		Potential flux
	F_{snow}	F_{ff}	F_{ice}[a]
FI1	–[b]	**+0.1 ± 0.1** (n=7)c	–[b]
FI2	**+0.4 ± 0.3** (n=13)[c]	–[b]	–[b]
FI3	**+0.1 ± 0.1** (n=7)[c]	–[b]	−0.6
FI4	**+0.1 ± 0.1** (n=6)[c]	–[b]	−0.8
FI5	**+0.6 ± 0.3** (n=5)[c]	–[b]	+2.6
FI6	**+0.2 ± 0.1** (n=5)[c]	–[b]	+11.8
FI7	**+0.1 ± 0.1** (n=10)[c]	–[b]	±0.0
YI1	–[b]	**+1.6 ± 0.2** (n=6)[c]	+7.3
YI2	–[b]	**+1.3 ± 0.2** (n=9)[c]	+1.0
YI3	–[b]	**+1.0 ± 0.4** (n=8)[c]	+1.1
OI1	**+0.1 ± 0.0** (n=6)[c]	–[b]	+0.2
Mean[d]	**+0.2 ± 0.2** (n=46)[c]	**+1.0 ± 0.6** (n=30)[c]	+2.5 ± 4.3 (n=9)[c]

a. Data of first measurement after removal of snow or frost flower.

b. "–" indicates no data.

c. Number of measurements in bracket.

d. Data of station OI1 was not included.